Chalcogenide Letters Vol. 19, No. 5, May 2022, p. 337 - 352

# Nickel sulfide nanoparticles on alumina and unsupported for *p*-chloroaniline production

A. Olivas[a,*], J. R. Rodríguez[b], F. Cardenas-Lizana[c], M. Cota-Leal[a], M. A. Keane[c]
[a]*Center for Nanosciences and Nanotechnology, National Autonomous University of Mexico (CNyN-UNAM), Carretera Tijuana-Ensenada- Km 107, CP 22860, Ensenada, B. C., México.*
[b]*PCeIM, CNyN-UNAM, Carretera Tijuana-Ensenada Km 107, CP 22860, Ensenada, B. C., México*
[c]*Chemical Engineering, School of Engineering and Physical Science, Heriot-Watt University, Edinburgh, EH 14 4AS, Scotland, United Kingdom*

Due to the need for producing intermediate chemicals such as *p*-chloroaniline (*p*-CA) using more environmentally friendly and efficient processes, nanostructured nickel and nickel sulfide-based catalysts were synthesized and studied. The selective p-chloronitrobenzene (*p*-CNB) gas-phase hydrogenation to produce *p*-CA was tested. The catalysts were characterized by $N_2$ physisorption ($S_{BET}$), temperature-programmed reduction (TPR), X-ray diffraction (XRD), scanning electron microscopy (SEM), energy dispersive X-ray spectroscopy (EDS), transmission electron microscopy (TEM), and X-ray photoelectron spectroscopy (XPS). The catalytic activity was evaluated in terms of conversion and selectivity towards *p*-CNB and *p*-CA, respectively. Based on the experimental results, the addition of sulfur promoted the selectivity towards *p*-CA in a range of temperature from 120 to 220 ºC. The selectivity towards *p*-CA was close to 100 %, avoiding the formation of undesirable side products. Therefore, it is suggested that sulfured-Ni based catalysts increase the surface acidity, which allowed improved hydrogenolysis of the N-O bond.

(Received January 26, 2022; Accepted May 10, 2022)

*Keywords:* Ni-based catalysts, Sol-gel method, Solvothermal method, p-chloronitrobenzene (p-CNB), Hydrogenation, p-chloroaniline (p-CA)

## 1. Introduction

Cleaner processes for the production of fine chemicals are important for contributing to a more environment-friendly chemical industry. A very valuable chemical intermediate such as *p*-chloroaniline (*p*- CA), is used to produce drugs, pesticides, herbicides, cosmetics, dyes, and other industrially useful products [1,2]. The acidic reduction of p- chloronitrobenzene (*p*-CNB) using Fe- based catalysts by means of Béchamp reaction is the main route to produce industrially *p*- CA [3]. However, a great quantity of toxic residues, which require expensive separation and disposal procedures are generated through Béchamp reaction [4]. Therefore, in a few years, this approach will not be feasible and reliable due to stricter environmental legislations [5,6]. In this sense, the scientific and industrial communities have made extensive research to obtain *p*- CA through clean processes as the *p*- CNB hydrogenation [7,8].

The hydrogenation of nitroarenes such as nitroaromatic chlorides can be well performed using heterogeneous catalysts such as transition- metal based catalysts [9,10]. In this context, Pt, Pd, Ni, or metal- alloys such as Pt- Rh and Ni- Mo [11–13] have been used as active phases. Active metals of p- CNB hydrogenation catalysts are usually metal oxides, metal- alloys, or completely reduced metals [1–3]. As well as, catalytic supports such as $Al_2O_3$, $SiO_2$, $Al_2O_3$-$SiO_2$, C, zeolites, and molecular sieves have been used for *p*- CNB hydrogenation [14,15]. Supported

* Corresponding author: ameliaolivas610@gmail.com
https://doi.org/10.15251/CL.2022.195.337

catalysts based on Pt, Pd, or Ni, usually synthesized by decomposition, impregnation, precipitation, co- precipitation, absorption, or ionic exchange methods, have shown good activity in *p*-CNB hydrogenation and selectivity towards *p*-CA [8]. The reaction mechanism of *p*-CNB hydrogenation has been scarcely reported in literature [14,16].

Ni- based catalysts have shown good activity, selectivity, and stability in hydrogenation and hydrodechlorination reactions [17–19]. It has been reported that $Ni/Al_2O_3$ improves the reduction of nitroaromatic chloride compounds and their derivatives in the gas-phase hydrogenation due to the electron-rich environment. The selectivity of $Ni/Al_2O_3$ towards *p*-CA production is higher at 120 ºC than at more elevated temperatures since high temperatures generate a large number of byproducts [14]. *p*-CA production can be inhibited by lateral undesired dehalogenation reaction due to hydrogenolysis reaction on the Cl-C bond in *p*-CNB [20]. Several factors, such as type of catalyst, solvent, support, temperature, and pressure, affect the dehalogenation reaction. The halonitrobenzene compounds with low halogen instability are less susceptible to dehalogenation reactions. It has been reported that palladium-based catalysts promote dehalogenation reactions [21]. Therefore, platinum, rhodium, iridium, ruthenium, and nickel are preferred as active metals [22]. Recent reports argue that sulfur addition improves the selectivity towards *p*-CA, although its effect is not well elucidated [23,24]. It has been established that platinum and cobalt sulfides present an elevated selectivity in the hydrogenation of the halonitrobenzenes, and these sulfides do not show dehalogenation reactions [25–27].

Ni-based catalysts have shown to be a good alternative for *p*-CNB hydrogenation. For example, the high selectivity of 90 % was reported towards *p*-CA with nickel Raney un-supported catalysts at 150 ºC using ethanol as solvent [28]. High selectivity values of 95 and 98 % towards p-CA at 150 ºC and 2 MPa of $H_2$ were obtained with sulfured-$NiMo/\gamma$-$Al_2O_3$ and sulfured-$CoMo/\gamma$-$Al_2O_3$ catalysts, respectively [29].

In this study we synthesized nanostructured Nickel and Nickel Sulfide supported and unsupported on alumina employing different methods as sol–gel and solvothermal. Their catalytic performance was tested in the *p*-CNB gas-phase hydrogenation for the clean production of *p*-CA using very low-cost Ni salts. To our knowledge, this research is a pioneering study on nanostructured Ni catalysts with sulfur as promoting element used in the *p*-CNB gas-phase hydrogenation. The obtained catalysts were characterized by $N_2$-physisorption ($S_{BET}$), temperature-programmed reduction (TPR), X-ray diffraction (XRD), scanning electron microscopy (SEM), energy dispersive spectroscopy (EDS), transmission electron microscopy (TEM), and X-ray photoelectron spectroscopy (XPS). The catalytic activity was discussed in terms of the conversion and selectivity of the initial *p*-CNB.

## 2. Experimental

### 2.1. Materials

Nickel (II) chloride ($NiCl_2 \cdot 6H_2O$, 99.98%), nickel (II) nitrate ($Ni(NO_3)_2 \cdot 6H_2O$, 99.98%), sodium thiosulfate pentahydrate ($Na_2S_2O_3 \cdot 5H_2O$, 99.99%), sodium hydroxide (NaOH, 99.9%), alumina ($Al_2O_3$, 99.9%), and ethanol ($C_2H_5OH$, 99.9%) were supplied by Alpha-Aesar; monohydrated hydrazine ($N_2H_4 \cdot H_2O$, 99%), *p*-chloronitrobenzene (*p*-CNB, 99.9%), methanol ($CH_3OH$, 99.9%), and butanol ($C_4H_9OH$, 99.5%) were acquired from Sigma-Aldrich.

### 2.2. Synthesis of the Ni-based catalysts

#### *2.2.1. Preparation of nano-nickel (M1)*

Auto-supported nano-nickel sample was prepared by the sol-gel method as it has been reported elsewhere [30]. An appropriate amount of hydrated nickel (II) chloride was dissolved in concentrated ethanol; afterward, $N_2H_4 \cdot H_2O$ solution (80% v/v) was added. Following, a NaOH solution was used for controlling the pH. The final solution was stirred for 6 hours and heated at 120 ºC, the black-colored precipitate was separated by centrifugation and dried at 70 ºC.

#### *2.2.2. Preparation of nickel sulfide (M2)*

Auto-supported nickel sulfide was prepared as it has been reported elsewhere by the solvothermal method [31]. An appropriate amount of hydrated nickel (II) chloride was dissolved in concentrated ethanol; afterward, $N_2H_4 \cdot H_2O$ (80% v/v) and $Na_2S_2O_3 \cdot 5H_2O$ solutions

were added. Following, a NaOH solution was used for controlling the pH. The final solution was stirred for 6 hours and heated to 120 ºC, the black-colored precipitate was separated by centrifugation and dried at 70 ºC.

***2.2.3. Preparation of nickel sulfide (M3)***.

Auto-supported nickel sulfide sample was prepared by the sol-gel method. An appropriate amount of hydrated nickel (II) chloride was dissolved in an $N_2H_4.H_2O$ solution (80% v/v); afterward, $Na_2S_2O_3 \cdot 5H_2O$ was added. The solution was stirred for 4 hours, the colloidal solution was placed in a Teflon reactor, where the reaction took place at 120 ºC for 6 hours, the black-colored precipitate was separated by centrifugation and dried at 70 ºC.

***2.2.4 Preparation of nickel/$Al_2O_3$ and nickel sulfide/$Al_2O_3$ (M4 and M5)***.

Two types of alumina–supported catalysts were prepared with a Ni loading of 5 wt. %. A Ni-based catalyst was prepared by incipient impregnation method [32], using T126 Gilder-alumina as support ($Al_2O_3$, 200 $m^2g^{-1}$, 0.365 $cm^3g^{-1}$ and 0.84 - 1.10 mm of average diameter). An appropriate quantity of $Ni(NO_3)_2 \cdot 6H_2O$ salt was dissolved in distilled water; afterward, the Ni solution was used to impregnate $Al_2O_3$ powders. The suspension was stirred in a rotary evaporator and heated at 70 ºC until water was completely evaporated. The obtained sample was dried at 120 ºC for 2 hours and calcined at 400 ºC for 4 hours. The gray-colored solid obtained was divided into two lots to have a control sample. One lot was reduced at 600 ºC using a $H_2$ flow for 1 hour; this sample was named $Ni/Al_2O_3$ (sample M4). The second lot was sulfured using a $H_2S/H_2$ mixture by the hydrothermal method at 400 ºC for 4 hours; the obtained black-colored solid was named $NiS_X/Al_2O_3$ (sample M5).

**2.3. Characterization of the support and catalysts**

The catalysts and support were characterized by $N_2$-physisorption in an Autosorb model, Quantachrome brand to determine the textural properties of the samples. The samples were degasified in air flow at 220 ºC for 2 hours prior to the analysis. Temperature- programmed reduction (TPR) was carried out on the M4 sample using a $H_2$/Ar mixture (5% $H_2$/Ar, v/v) with a flow of 12 $cm^3min^{-1}$ in a desorption equipment, model Multipulse RIG of ISRI, equipped with a thermal conductivity detector (TCD). The TPR analysis was performed from 20 ºC to 600 ºC with a heating rate of 5 ºC $min^{-1}$. The quantity of $H_2$ consumed was obtained by the integration of the peaks of the TPR profile using a standard procedure included in the software of the Multipulse RIG unit.

To determine the crystallinity of the samples, X-ray diffraction (XRD) was performed using a powder X-ray diffractometer, Philips X'perts with Cu Kα radiation. The XRD patterns were registered in an angular range 2θ from $20^{\circ}$ to $80^{\circ}$. Scanning electron microscopy (SEM) was performed to determine the surface characteristics of the samples in a JEOL 5300 (JSM-5300) microscope using secondary electrons at an energy interval of 0 – 50 eV. Transmission electron microscopy (TEM) was performed on a JEOL-2010 (JTM-2010) microscope at 200 kV.

To determine the chemical state on the catalysts, X-ray photoelectron spectroscopy (XPS) was performed in a laser ablation system, Riber LDM-32 with an acceleration potential of 12 kV at 30 mA. The XPS equipment was coupled with an electron analyzer type CAMECA, model MAC-3.

The catalytic activity tests for the *p*-CNB hydrogenation reaction were carried out in a microreactor operated in a dynamic regimen at atmospheric pressure under differential conditions [33–35], at 120, 120, 140, 160, 180, and 220 ºC. The temperature of the reaction was continually monitored using a thermocouple to maintain a constant temperature. The catalyst amount in every catalytic test was 500 mg diluted in glass dust (75 μm).

Borosilicate balls (D = 1 mm) were used for packing the reactor and were located in the pre-heating zone which avoided the evaporation of reactants and allowed a homogeneous mixing. The gas-phase reactants were fed to the reactor through a Teflon line using a microprocessor to control flow velocity (scientific model 100 kd) and was monitored using a digital flow meter (model Humonics 520). Hydrogen was fed with a 95 % excess of the stoichiometrically required

amount with a GHSV = $2x10^4$ $h^{-1}$, and *p*-CNB was fed with a modular aromatic injection flow of 1.2 mmol $h^{-1}$. The effluent of the reactor was cooled with a liquid-$N_2$ trap to be analyzed at intervals of 20 - 30 minutes for 5 hours. The products and reactants were analyzed by gas chromatography in a Perkin-Elmer auto-system XL system (auto-sampler) with capillary column (J&W Scientific, 50 m x 0.20 mm) coupled to a flame ionization detector. In this study, only were obtained *p*-CA and aniline (AN) as reaction products. The uncertainty analysis of the experimental procedure was carried out taking into account the calibration process of the different equipment, deviation values by the manufacturer and standard deviation of the different measurements. The uncertainty was expressed as standard uncertainty for the different measurements made in this research work.

The catalytic activity was discussed in terms of *p*-CNB conversion and *p*-CA selectivity. The conversion was defined as the amount of change of *p*-CNB, at any time, relative to the initial amount of *p*-CNB fed, and the selectivity was determined as the amount of a specific product relative to the amount of all reaction products. The conversion and selectivity were defined by the following equations (1) and (2):

$$Conversion\ (\%) = \frac{mol_{p-CNB}reacted}{mol_{p-CNB}initial} * 100 \quad (1)$$

$$Selectivity\ (\%) = \frac{mol_{p-CNB}generated}{\sum mol_{p-CNB}initial} * 100 \quad (2)$$

## 3. Results and discussion

### 3.1. Results

The X-ray diffraction patterns of the synthesized materials are shown in Figure 1. It can be observed that the XRD diffractogram for M1 shows the main diffraction peaks corresponding to high-purity metallic Ni (JCPDS 04-0850). The XRD diffractograms of M2 and M3 show the diffraction peaks corresponding to the sulfured-Ni phase on the samples. The diffraction peaks can be assigned to the presence of NiS (JCPDS 12-0041) and $Ni_9S_8$ (JCPDS 78-1886) in the M2 and M3 samples, respectively. For the M4 and M5 samples, it was not possible to observe the characteristic peaks of Ni or $NiS_x$. In these samples, the XRD patterns were characteristic of amorphous $Al_2O_3$.

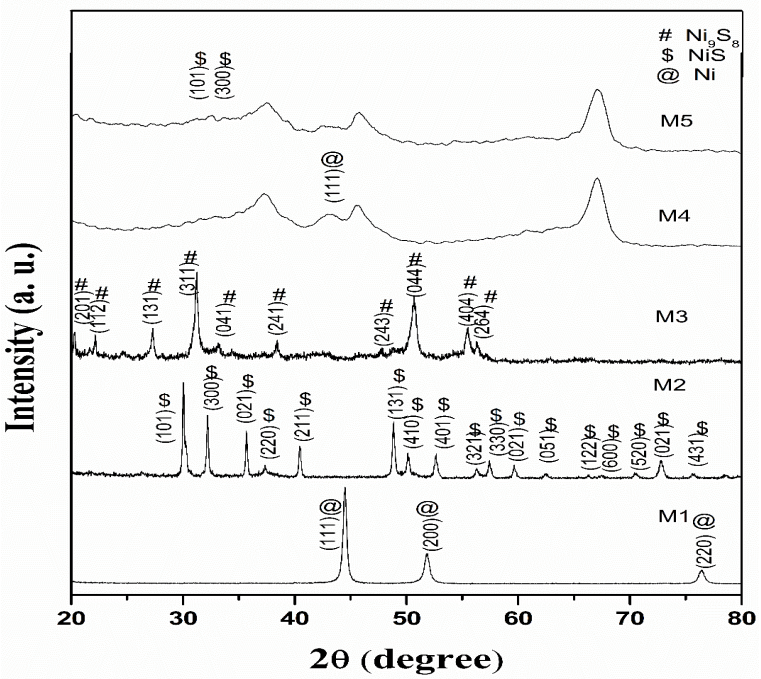

*Fig. 1. XRD diffractogram patterns of the synthesized materials.*

The crystal size of the catalysts was calculated through the Scherrer equation using the XRD signals corresponding to the planes (111) of Ni for M1, (101) of NiS for M2, and (311) of $Ni_9S_8$ for M3. The crystal size of M4 and M5 samples were calculated by a TEM statistical particle analysis. The average crystal size of the samples is presented in Table 1. It can be observed that crystal size changes in relation to the synthesis method, from 3 to 85 nm. The higher crystal size corresponds to the auto-supported samples which were synthesized by sol-gel and solvothermal method. The supported samples had smaller crystal size compared with the un-supported samples. Also, the surface area of the samples is shown in Table 1. It can be observed that surface area of un-supported samples is smaller than the surface area of supported samples. Therefore, the crystal size is smaller to the supported samples due to the largest surface area available to be deposited. In contrast, the higher crystal size of un-supported samples is due to the active phases (crystallites) belong to the matrix of the sample.

*Table 1. Average size and surface area of the synthesized materials.*

| Sample | Surface area ($m^2g^{-1}$) | Average size crystal (nm) |
|---|---|---|
| M1 | 2.5 ± 0.9 | 40 ± 2 |
| M2 | 3.1 ± 1 | 70 ± 4 |
| M3 | 2.3 ± 0.8 | 85 ± 6 |
| M4 | 171 ± 4 | 3 ± 0.2 [a] |
| M5 | 119 ± 5 | 10 ± 0.6 [a] |
| [a] *Average size values determined by TEM analysis* | | |

Figure 2 shows the TPR profile analysis for the activation of the catalyst M4. Two reduction peaks can be observed at 324 and 597 ºC.

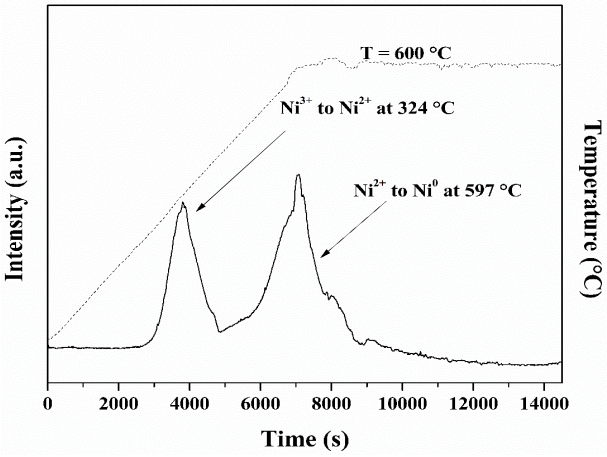


*Fig 2. TPR profile of the M4 sample.*

The first reduction peak at 324 ºC corresponds to the reduction of the $Ni^{3+}$ species to $Ni^{2+}$ species. The high-temperature reduction peak was assigned to the reduction of the $Ni^{2+}$ species to $Ni^0$ species (metallic nickel) [16]. The total $H_2$ uptake was 4 µmol of $H_2g^{-1}$. According to the mass used to the reduction treatment, the above analysis could suggest that the preponderant species on the catalytic support are $Ni^0$ species.

Figure 3 shows the SEM micrographs of M1-M5 samples. M1 and shows spherical surface structure with a diameter of ~ 50 nm ± 3 which corresponding to metallic Ni. M2 sample shows a

bar-shaped structure with different endings, but with mostly squared endings which is characteristic of NiS, the average length of these bars was 4 µm ± 0.2 and 1 µm ± 0.04 width.

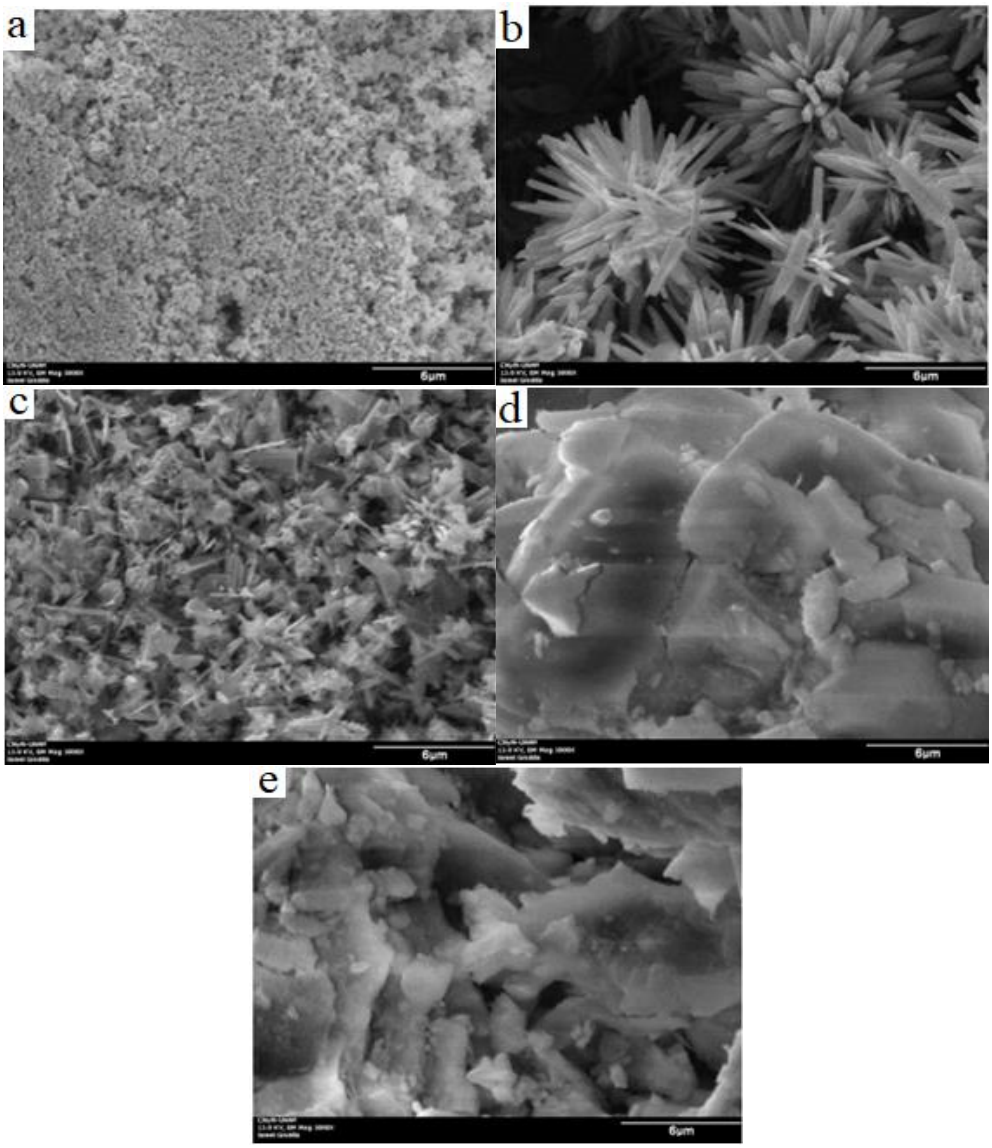


*Fig 3. SEM micrograph of the a)M1, b)M2, c)M3, d)M4 and e)M5.*

The M3 sample exhibits the $Ni_9S_8$ structure with irregular shapes and sizes less than 6 µm but characteristic of sulfured samples. $Ni/Al_2O_3$ particles correspond to M4 sample with a non-homogeneous surface and without a defined shape. Finally, M5 sample present compact particles of $NiS_X/Al_2O_3$ with an irregular topography on its surface. The structure or shape of the particles on un-supported samples (M1, M2 and M3) presented a more defined shape than the supported samples (M4 and M5). It can be observed that the structure or the shape of the particles on the catalytic surface was different according to the preparation method.

Figure 4 shows the TEM micrographs and electron diffraction pattern for M1-M5 samples. Figure 4(a,b) shows the TEM micrograph and diffraction pattern of the M1 sample. Spherical uniform-size particles can be observed with an average diameter of 55 nm ± 3.

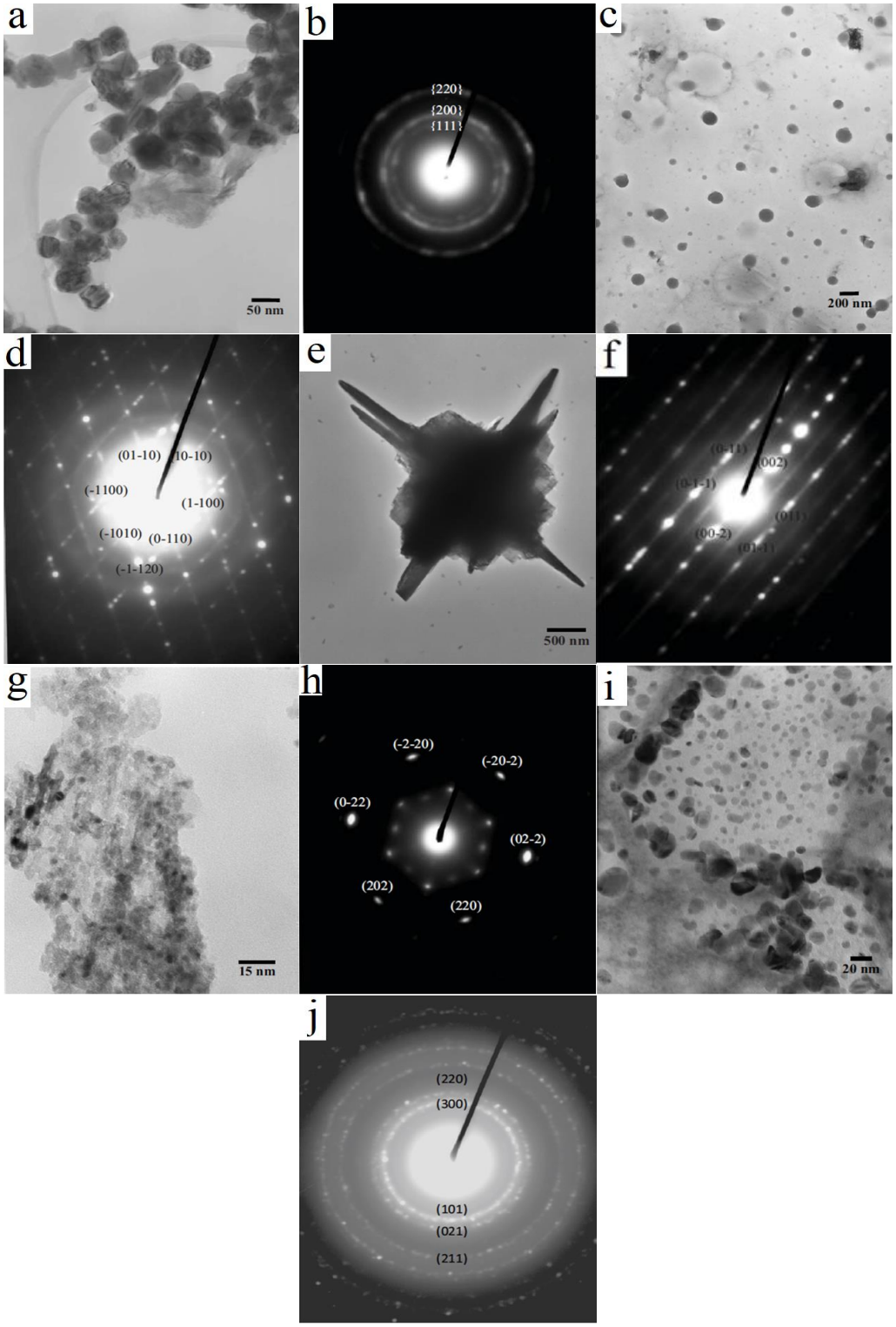


*Fig 4. TEM micrograph and diffraction pattern of the M1(a,b), M2(c,d) M3(e,f) M4(g,h) M5(i,j).*

The diffraction pattern shows three rings which belong to the (111), (200), and (220) planes. These rings were assigned to a face-centered cubic structure (FCC) of the metal Ni. M2 sample presented spherical particles of variable diameters up to ~150 nm ± 8. The diffraction pattern presents a series of spots and lines that form hexagons. The spots belong to a specific plane, depending on its inter-planar distance. The indexed planes were: (1−100), (0−110), (−1−120), (−1010), (−1100), (01−10), and (10−10). These planes belong to the trigonal structure

of NiS, which is observed from direction [001]. Figure 4(e,f) shows the TEM micrograph and diffraction pattern of the M3 sample. The sample shows large crystals with particles smaller than ~ 60 nm. The diffraction pattern presents a series of spots and lines that form rectangles centered in two facets and the center. The signals were assigned to an orthorhombic structure centered around the base, which is observed from direction [100] giving the following planes: (011), (01−0), (0−1-1), (0−11), (002), and (00−2). These planes belong to the structure of synthesized $Ni_9S_8$. Figure 4(g,h) shows the TEM micrograph and TEM diffraction pattern of M4. The material was formed by spherical particle conglomerations of uniform size with an average diameter of 3 nm ± 0.2. The TEM diffraction pattern of the material was indexed considering the inter-planar distance, intensity of the spots, and angles between them. The assigned planes were the following: (220), (202), (02−2), (−2-20), (−20−2), and (0−22), which belong to the family of equivalent planes {220} and were observed from the direction [11−1]. The other spots belong to the {110} and {200} family planes. Finally, The TEM micrograph and electron diffraction pattern of the M5 sample shown spherical particles of irregular size with an average diameter of 10 nm ± 0.5. In the diffraction pattern, six rings of high and two of low intensity can be observed. The rings were indexed depending on the inter-planar distance and their intensity. The family of equivalent planes presented are: {101}, {300}, {012}, {220}, and {211}, which are characteristic of NiS. The above analysis suggested that metallic nickel is the main specie on the catalytic support to M4 sample. TEM micrographs and TEM diffraction patterns results agree with previous XRD, SEM and TPR results about the crystal size and with the phase assignment of all samples. The preparation method was the preponderant factor to determine the structure, shape and size of the particles. Additionally, the supported and the un-supported samples showed an important difference in the textural properties. All above characteristics will determine the catalytic performance of the samples tested in the p-CNB hydrogenation to obtain p-CA as the desired product.

The survey and high-resolution spectra of all samples are show in fig. 5,6,7, 8 and 9. In the spectrum of auto-supported Ni (M1), five transitions can be observed. The transitions at a binding energy of 886 and 904 eV are the transitions of Ni $2p_{3/2}$ and Ni $2p_{1/2}$ orbitals that are assigned to $Ni^0$, and the other three transitions suggest the existence of $Ni^{2+}$ present as oxide, which causes the formation of signals by shake-up. Since the area of the peaks corresponding to $Ni^0$ was higher (2 times) than that corresponding to $Ni^{2+}$ on M1, and as the catalyst was tested immediately after its synthesis, $Ni^0$ species was supposed to be the only specie present. The spectrum of un-supported sulfured-Ni (M2) shows three transitions. The transition at 886 eV binding energy corresponds to Ni $2p_{1/2}$ transition and was assigned to $Ni^{2+}$ species. Also, there was determine the presence of sulfur at 180 eV corresponds to $S^{2-}$ species. Since S was present in the M2 sample (sulfured-Ni), we assume that the transition of Ni at a binding energy of 892 eV corresponds to the presence of a shake-up [36,37]. The spectrum of unsupported sulfured-Ni (M3) shows four transitions. The transitions at a binding energy of 860 and 877 eV correspond to Ni $2p_{3/2}$ and Ni $2p_{1/2}$ orbitals, respectively, which indicated the presence of $Ni^{2+}$ species. The presence of $S^{2-}$ species was corroborated by the transitions at a binding energy of 168 and 174 eV. A shake-up was observed at 866 and 883 eV as in the previous samples. The spectrum of supported Ni (M4) shows two transitions. The transition at a binding energy of 869 eV corresponds to Ni $2p_{3/2}$ orbital, which indicates the presence of $Ni^0$ species supported on $Al_2O_3$. The transition at a binding energy of 875 eV corresponds to the shake-up. Also, the Al $2p_{1/2}$ and O $1s_{1/2}$ transitions at a binding energy of 86 and 544 eV corresponding to the presence of Al and O of the $Al_2O_3$ can be observed. Figure 9 shows the low and high-resolution spectra of the M5 sample. Supported sulfured-Ni (M5) shows four transitions. The transitions at a binding energy of 867 and 884 eV correspond to Ni $2p_{3/2}$ and Ni $2p_{1/2}$ orbitals which confirmed the presence of $Ni^{2+}$ species. The S 2p transition at 173 eV can be observed, which indicated the presence of S species related to a $NiS_x$. The transitions at 873 and 891 eV were due to the presence of a shake-up. The presence of O and Al of $Al_2O_3$ was confirmed by the Al $2p_{1/2}$ and O $1S_{1/2}$ transitions at a binding energy of 85 and 542 eV, respectively.

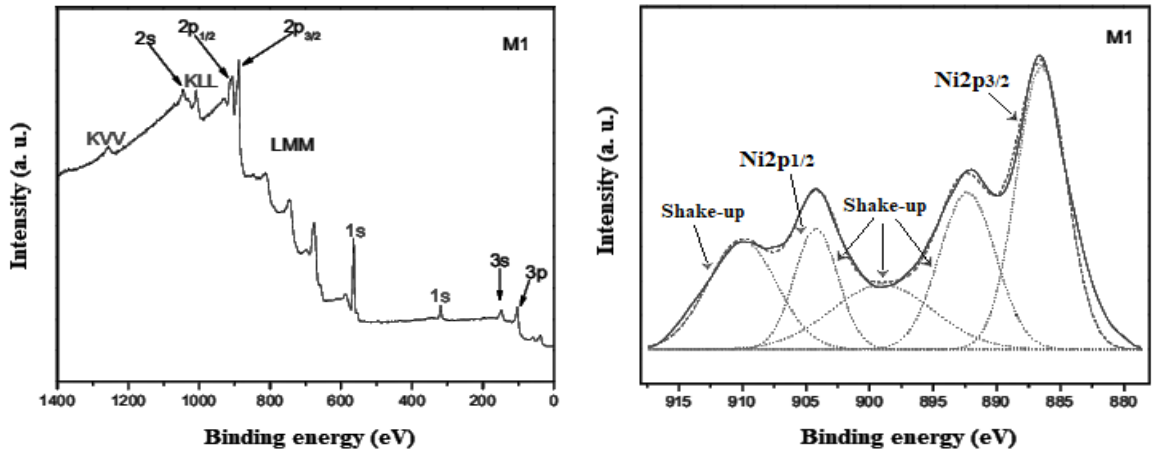


*Fig. 5. Survey and high-resolution XPS spectra of the M1 sample.*

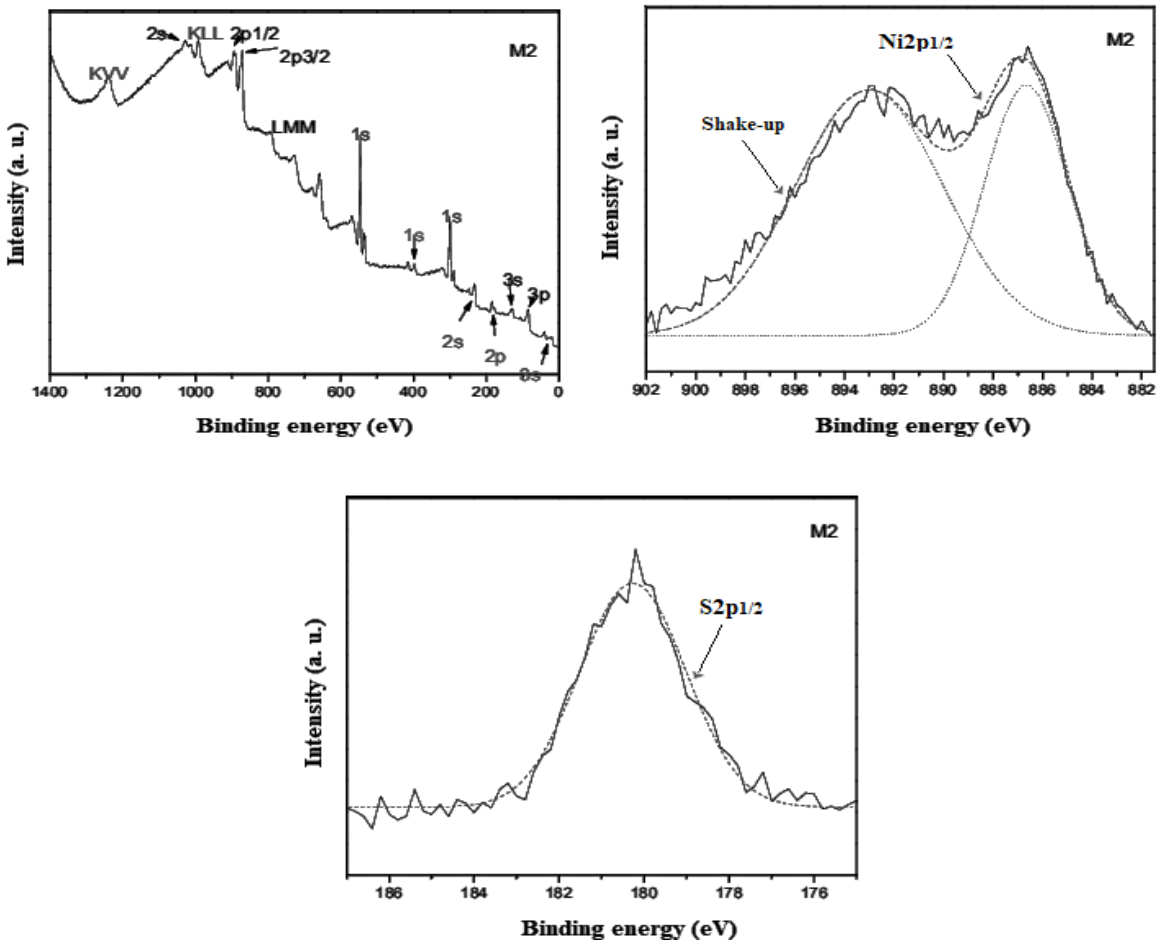


*Fig. 6. Survey and high-resolution XPS spectra of the M2 sample.*

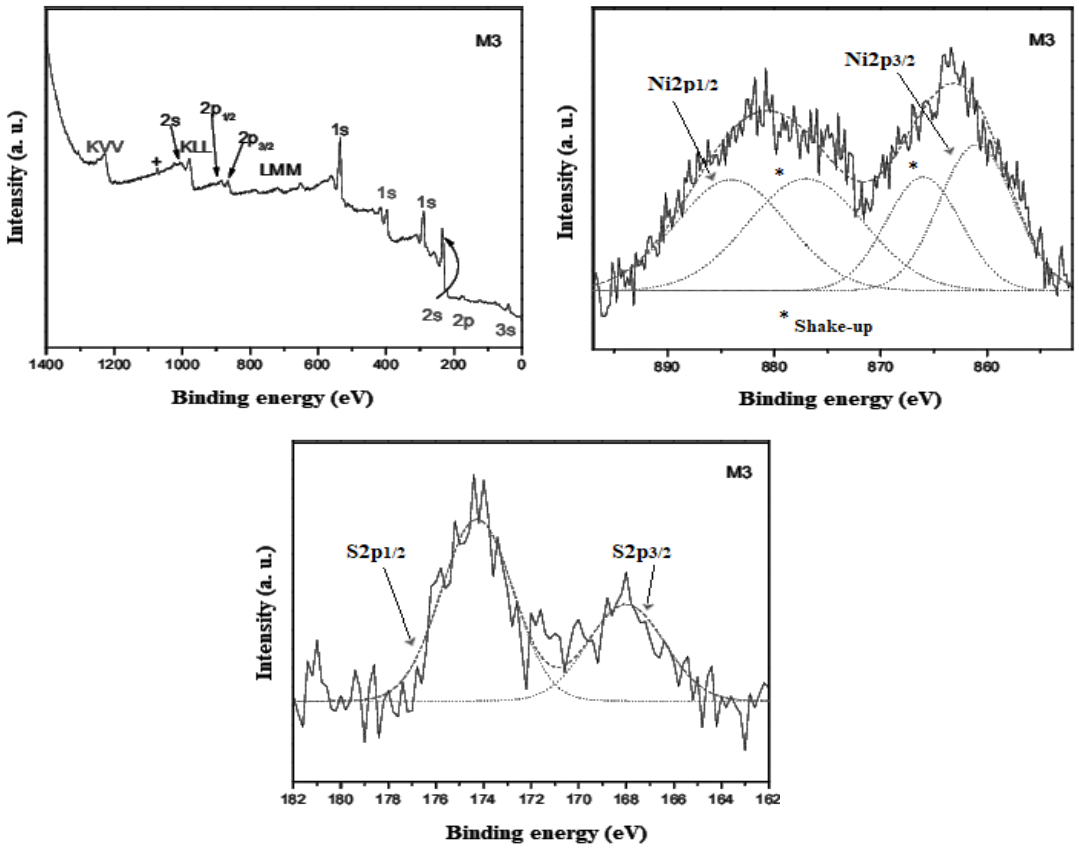


*Fig. 7. Survey and high-resolution XPS spectra of the M3 sample.*

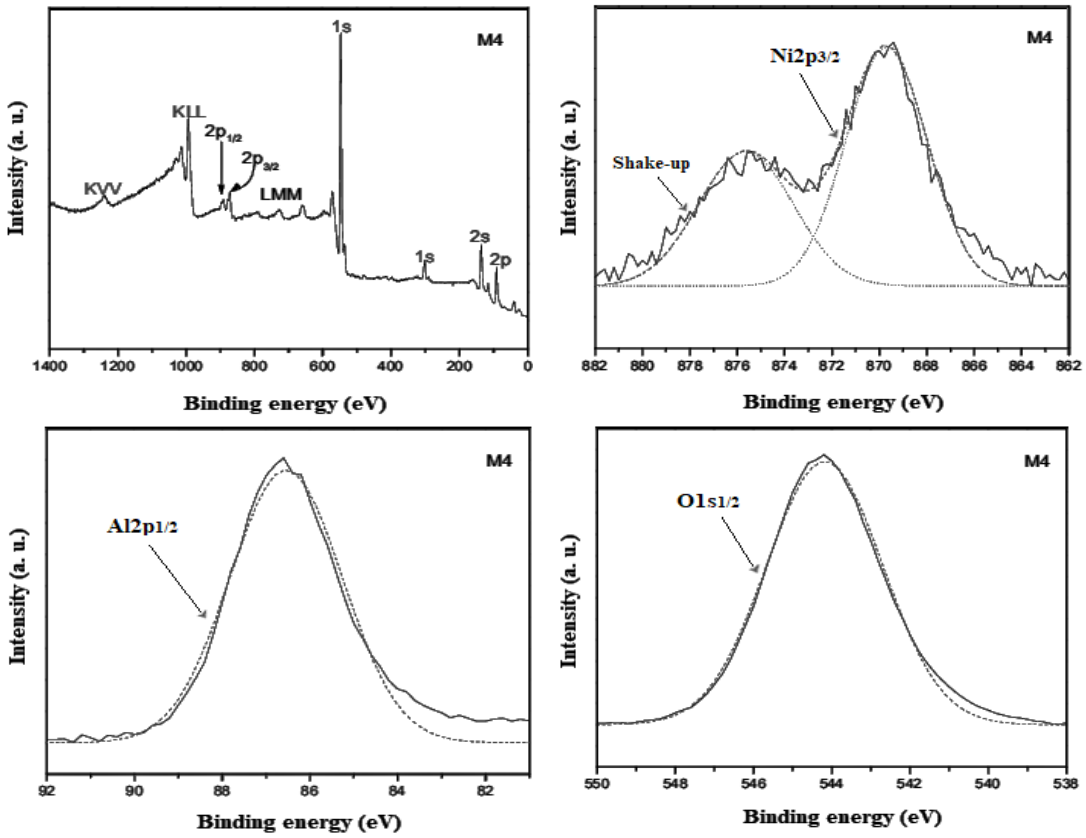


*Fig. 8. Survey and high-resolution XPS spectra of the M4 sample.*

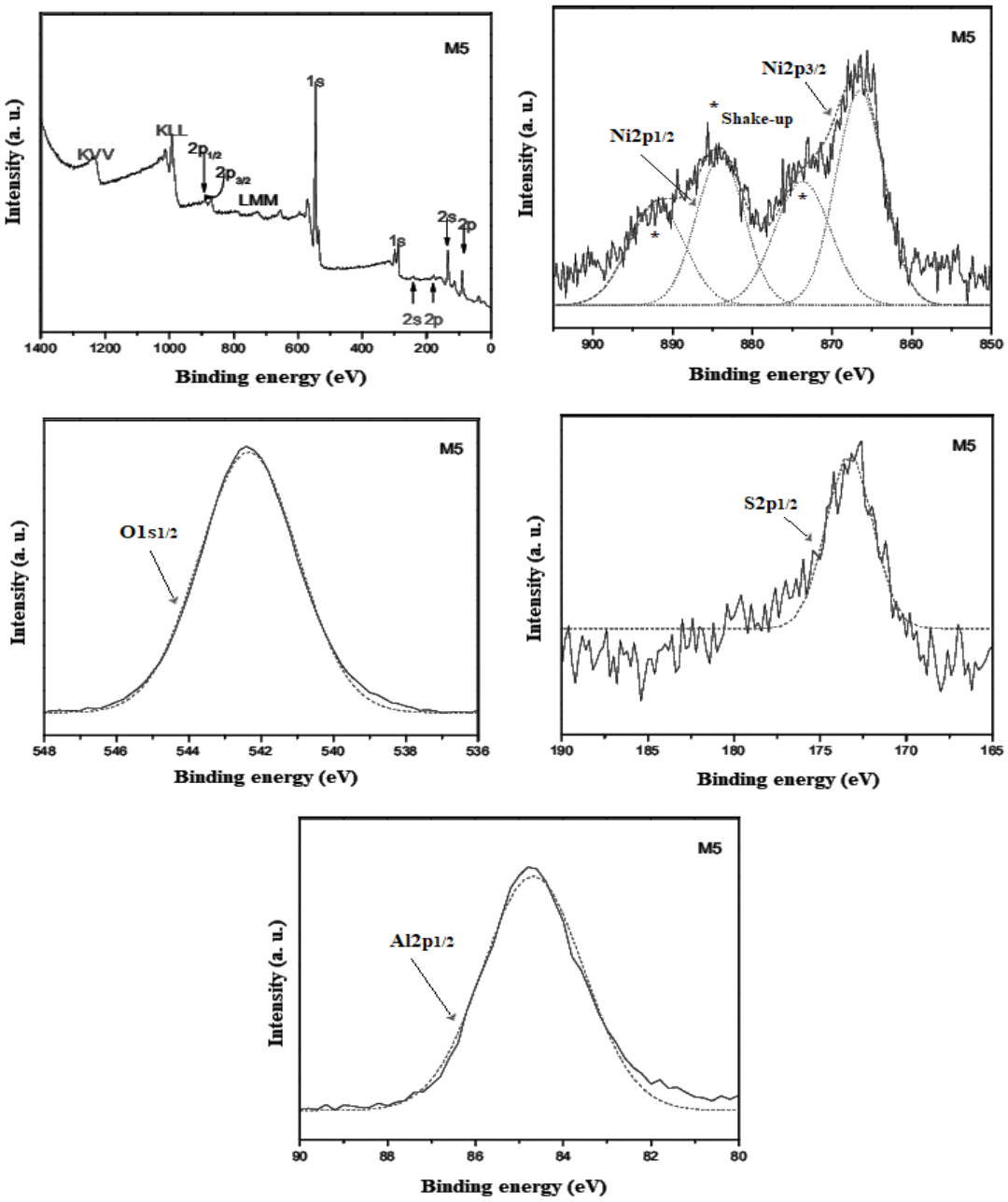


*Fig. 9. Survey and high-resolution XPS spectra of the M5 sample.*

Table 2 shows the X- ray photoelectron spectroscopy quantitative results.

*Table 2. X- ray photoelectron spectroscopy (XPS) results.*

| | M1 | M2 | M3 | M4 | M5 |
|---|---|---|---|---|---|
| Element | Atomic ratio (%) | | | | |
| Ni | 98 ± 5.0 | 48.4 ± 2.5 | 51.3 ± 2.6 | 4.9 ± 0.3 | 4.4 ± 0.2 |
| S | - | 47.6 ± 2.5 | 45.7 ± 2.4 | - | 4.7 ± 0.2 |
| Al | - | - | - | 36.0 ± 2.8 | 29.8 ± 1.5 |
| O | - | - | - | 59.1 ± 3 | 61.1 ± 3.0 |

The XPS spectra were decomposed by deconvolution to determine the atomic concentrations of the species. The deconvolution of the signals was performed considering the orbital transitions of Ni $2p_{3/2}$, S $2p_{1/2}$, Al $2p_{1/2}$, $O1s_{1/2}$. Also, the sensibility factors (S) were calculated in function of the binding energy (BE) for the above-mentioned transitions of each element.

The XPS results allow to corroborate the findings using the other physical-chemical characterizations since the surface atomic contents are agree with the phase assignment made previously. Also, the XPS results suggest the correct synthesis method of the samples since the expected species were present and therefore a properly comparison of the catalytic performance can be made between the different samples.

Figure 10 shows the conversion and selectivity results for the different Ni and sulfured-Ni samples in the *p*- CNB gas- phase hydrogenation reaction in a temperature range from 120 to 220 ºC during 5 hours of reaction time. It can be observed that the conversion of *p*- CNB increases at higher temperature for all samples. Furthermore, it can be observed that the M1 and M4 sample reach a high conversion value beginning at low temperatures. On the other hand, the selectivity towards *p*- CA was close to 100 % at 120 ºC for all samples, and only the M2 and M5 samples present high values of selectivity towards *p*- CA at high temperatures.

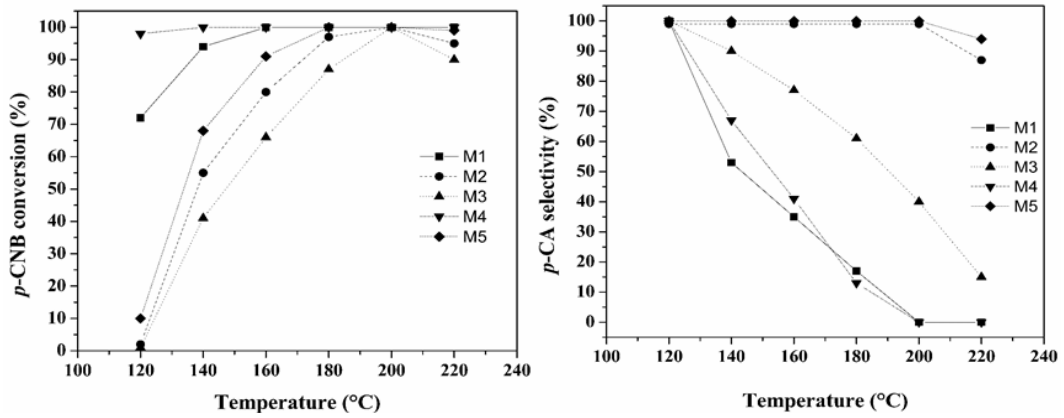


*Fig. 10. Conversion and selectivity results of the samples.*

### 3.2. Discussion

According to the crystallographic database JCPDS-ICDD, the XRD patterns of the unsupported Ni catalyst (M1) and unsupported sulfured-Ni (M2 and M3) catalysts (see Figure 1) show the presence of Ni, NiS, and $Ni_9S_8$, respectively, on their surfaces. The XRD patterns of supported Ni (M4) and supported $NiS_x$ (M5) catalysts could not be assigned to any characteristic compound. These above results were probably due to the average particle sizes of 3 and 10 nm for M4 and M5, respectively (by TEM analysis). Therefore, the amorphous $Al_2O_3$ generates noise in the XRD patterns. Also, the TEM diffraction patterns of the catalysts (Figure 4(h,j)) confirmed the active phases of M4 and M5 to be metallic Ni/Ni oxide and NiS, respectively.

Figure 2 shows the TPR profile analysis obtained for the activation of the supported Ni catalyst (M4). The reduction peak at 324 ºC was assigned to the interaction between Ni and oxygen in the different types of Ni oxides [16,38,39]. The high-temperature reduction peak at 597 ºC was assigned to the strong interaction between different types of Ni and $Al_2O_3$ oxides [39]. These characteristic reduction peaks have been assigned to a spinel-type $NiAl_2O_4$ on the surface [39–41]. This last observation could explain the presence of Ni oxide on the supported Ni catalyst (M4).

According to the XRD (Figure 1) and TEM results (Figure 4), the average crystallite size of the un-supported catalysts was greater than supported catalysts. The average crystallite size of the un-supported Ni catalyst (M1) was 50 nm, while the average crystallite size of the supported Ni catalyst (M4) was 3 nm. Similarly, the un-supported sulfured-Ni catalyst (M2) had an average

crystallite size of 70 nm, while the supported $NiS_x$ catalyst (M5) had an average crystallite size of 10 nm. Sulfur concentration also influenced a larger average crystallite size. Average crystallite sizes of un-supported Ni catalyst (M1) and un-supported sulfured-Ni catalysts with 11 % difference in sulfur amount (M2 and M3 samples) were 50, 70, and 85 nm, respectively. According to the surface area results (Table 1), the increase of the average crystallite size promoted the decrease of surface area. The largest crystallite average size (85 nm) of un-supported sulfured-Ni catalyst (M3) had the smallest value of surface area (2.3 $m^2g^{-1}$). The smallest average crystallite size (3 nm) of supported Ni catalyst (M4) had the largest surface area value (171 $m^2g^{-1}$), as expected.

Figures 3 show the SEM micrographs of the catalysts. It can be observed that the morphology of the samples was very different. Un-supported Ni catalyst (M1) show spherical-shape particles, un-supported sulfured-Ni (M2) present bar-shape particles, un-supported sulfured-Ni (M3) show a sheet-shaped structure, and finally, supported Ni (M4) and supported $NiS_x$ (M5) did not present an apparent shape, they appeared as piling layers. It could be observed that the composition of the catalysts was important to determine the characteristic structure and morphology of the material. Therefore, these characteristics will largely determine the catalytic activity.

According to the Figure 10, it can be observed that *p*-CA was the only detected product at 120 ºC for all samples. At 200 ºC, *p*-CA and AN were detected as reaction products. The product distribution was different for the sulfured and non-sulfured samples. The non-sulfured nickel samples (M1 and M4) shown greatest amount of AN as reaction product while sulfured-Ni samples (M2, M3 and M5) shown a largest amount of *p*-CA as reaction product. These results indicated that sulfur addition promoted the selectivity towards *p*-CA even at high temperature. At 200 ºC the most selective catalyst was M2 (un-supported NiS) followed by M5 (supported NiS). The un-supported NiS was twelve-fold more active than supported NiS. Therefore, it could be inferred that more amount of NiS exposed or a better distribution on the catalytic support should improve the selectivity towards *p*-CA.

Base on the conversion of *p*-CNB hydrogenation at different it can be observed that *p*-CNB conversion rises at higher temperatures for all materials (figure 10). Unsupported Ni (M1) and supported Ni (M4) were the more active catalysts in the p-CNB conversion. Conversion of 70 % of p-CNB was reached by M1 at 120 ºC and rose up to ~ 99.9 % at 220 ºC. M4 showed ~ 93 % conversion of *p*-CNB at 120 ºC and reached ~ 99.9 % at 220 ºC. The other catalysts rose the *p*-CNB conversion proportionally at high temperatures. But it could be observed that the catalysts with high conversion values from 120 ºC were not the more selective catalysts towards *p*-CA at higher temperature. For all catalysts, selectivity towards p-CA at 120 ºC was ~ 99.9 %. The above results agree with Cárdenas-Lizana *et al*. who reported p-CA as the only product in the *p*-CNB gas-phase hydrogenation over $Ni/Al_2O_3$ catalysts at 120 ºC [16]. Only supported and unsupported sulfured-Ni catalysts (M2 and M5) maintained high selectivity at higher temperatures. M1, M3, and M4 lowered *p*-CA selectivity at higher temperatures. Based on these results, the addition of sulfur allowed the selectivity to be kept towards *p*-CA even at high temperatures. Supported sulfured-Ni catalyst showed the best selectivity towards *p*-CA, followed by un-supported sulfured-Ni catalyst. According to the results, it can be observed that the selectivity was maintained even at high temperatures, for those samples containing nickel sulfide. Oudar *et al*. stated that chemisorbed sulfur over Ni monocrystals causes an electron-transfer from Ni to S which generates greater number of active sites [42]. The increase in the electron density on the surface increases the surface acidity and favors the bonding between hydrogen atoms, creating acidic sites S-H. The high selectivity towards *p*-CA can be explained due to the hydrogenolysis of the N-O bond promoted by the Ni and S-H acidic sites. According to the XPS results (Table 2), it could be suggested that hydrogenolysis was only due to the Ni metallic sites for supported and un-supported Ni catalysts (M1 and M4) and the by acidic sites (S-H) for supported and un-supported NiS catalysts (M2 and M5). Also, the hydrogenolysis of N-O bonds could be caused by both the Ni metallic and acidic sites on un-supported sulfured-Ni catalyst prepared by the solvothermal method (M3). The breaking of the N-O bonds due to acidic sites involves a consecutive attack of a proton towards nitrogen and oxygen, eliminating water. Afterward, the protons are easily

recovered on the surface due to the large excess of hydrogen in the reaction. Based on the above results, it could be proposed that the inferior- facet acidic sites of the NiS crystals (trigonal structure as established above) promoted high selectivity towards *p*-CA in a wide range of temperatures according to the method of catalyst preparation. This research proposes new insight about the role of the sulfur to enhance the clean production and *p*-CA selectivity by means of the *p*-CNB hydrogenation using sulfured-Ni catalysts, even at high temperature when it became necessary.

## 4. Conclusions

Nanostructured sulfured- Ni and Ni catalysts were synthesized to be tested in the hydrogenation of p-chloronitrobenzene (p-CNB) to selectively produce p-chloroaniline (p-CA) within a temperature range from 120 to 220 ºC. The experimental results showed the presence of metallic Ni on the Ni catalysts and NiS and $Ni_9S_8$ species on the sulfured-Ni catalysts. Sulfured-Ni catalysts presented a better selectivity towards p-CA production at high temperatures, while Ni catalysts significantly decreased the p-CA selectivity. The high selectivity of sulfured-Ni catalysts was close to 100 % and was maintained in the experimental temperature range (120 – 200 ºC). According to the results, it could be suggested that the presence of NiS crystallites promotes the formation of acidic sites S-H, which allow better hydrogenolysis of the N-O bond, and therefore favors p-CA formation. Hence, sulfured-Ni catalysts are an adequate option to selectively produce p-CA in a cleaner and environmentally friendly process. The catalysts presented satisfactory results, but the sulfurized sample not supported in alumina (M2) and the metal nickel sample supported in alumina (M4) are the ones that presented the best results with characteristic properties. This gives us a range of possibilities for adaptation towards an environmentally friendly hydrogenation system for the production of p-CA.

### Acknowledgments

We thank F. Ruíz, E. Aparicio, I. Gradilla and G. Soto for the technical assistance (HRTEM, XRD, SEM-EDX and XPS respectively). We are grateful with M.Sc. F. Aguilera by grammar and spelling revision. M. Cota-Leal gratefully acknowledges the postdoctoral grant from the program DGAPA-UNAM. This work was supported by the Project IN107220 from DGAPA-PAPIIT, UNAM. J. R. Rodríguez thanks to CONACyT scholarship.

## References

[1] P. Gupta, S. Paul, Solid acids, Catal. Today. 236, 153 (2014); https://doi.org/10.1016/j.cattod.2014.04.010

[2] M. Burgman, M. Tennant, N. Voulvoulis, K. Makuch, K. Madani, Curr. Opin. Green Sustain. Chem. 13, 130 (2018); https://doi.org/10.1016/j.cogsc.2018.04.006

[3] H. Cheng, X. Meng, Q. Wang, J. Ming, Y. Yu, F. Zhao, J. Colloid Interface Sci. 377, 322 (2012); https://doi.org/10.1016/j.jcis.2012.03.042

[4] M. Irfan, T.N. Glasnov, C.O. Kappe, ChemSusChem. 4, 300 (2011); https://doi.org/10.1002/cssc.201000354

[5] H.-U. Blaser, H. Steiner, M. Studer, ChemCatChem. 1, 210 (2009); https://doi.org/10.1002/cctc.200900129

[6] J. Song, Z.-F. Huang, L. Pan, K. Li, X. Zhang, L. Wang, J.-J. Zou, Appl. Catal. B Environ. 227, 386 (2018); https://doi.org/10.1016/j.apcatb.2018.01.052

[7] P. Serna, A. Corma, ACS Catal. 5, 7114 (2015); https://doi.org/10.1021/acscatal.5b01846

[8] D.-S. Lee, Y.-W. Chen, Chinese J. Catal. 34, 2018 (2013); https://doi.org/10.1016/S1872-

2067(12)60687-1
[9] H. Yu, W. Tang, K. Li, H. Yin, S. Zhao, S. Zhou, Chem. Eng. Sci. 196, 402 (2019); https://doi.org/10.1016/j.ces.2018.11.024
[10] X. Cui, X. Zhou, Z. Dong, Catal. Commun. 107, 57 (2018); https://doi.org/10.1016/j.catcom.2018.01.015
[11] A.F. Sierra-Salazar, V. Hulea, A. Ayral, T. Chave, S.I. Nikitenko, P.J. Kooyman, F.D. Tichelaar, S. Abate, S. Perathoner, P. Lacroix-Desmazes, Microporous Mesoporous Mater. 256, 227 (2018); https://doi.org/10.1016/j.micromeso.2017.08.016
[12] P. Zhang, Y. Hu, B. Li, Q. Zhang, C. Zhou, H. Yu, X. Zhang, L. Chen, B. Eichhorn, S. Zhou, ACS Catal. 5, 1335 (2015); https://doi.org/10.1021/cs501612g
[13] F. Cárdenas-Lizana, Y. Hao, M. Crespo-Quesada, I. Yuranov, X. Wang, M.A. Keane, L. Kiwi-Minsker, ACS Catal. 3, 1386 (2013); https://doi.org/10.1021/cs4001943
[14] S. Li, X. Chen, J. Wang, N. Yao, J. Wang, J. Cen, X. Li, Appl. Surf. Sci. 489, 786 (2019); https://doi.org/10.1016/j.apsusc.2019.05.366
[15] C. Su, X.-N. Li, Q.-F. Zhang, L. Ma, C.-S. Lu, F. Feng, Chinese Chem. Lett. 24, 59 (2013); https://doi.org/10.1016/j.cclet.2012.12.006
[16] F. Cárdenas-Lizana, S. Gómez-Quero, C. Amorim, M.A. Keane, Appl. Catal. A Gen. 473 41 (2014); https://doi.org/10.1016/j.apcata.2014.01.001
[17] L. Huang, Y. Lv, S. Wu, P. Liu, W. Xiong, F. Hao, H. Luo, Appl. Catal. A Gen. 577, 76 (2019); https://doi.org/10.1016/j.apcata.2019.03.017
[18] L. Lang, Z. Pan, J. Yan, J. Alloys Compd. 792, 286 (2019); https://doi.org/10.1016/j.jallcom.2019.03.323
[19] G. Romanazzi, A.M. Fiore, M. Mali, A. Rizzuti, C. Leonelli, A. Nacci, P. Mastrorilli, M.M. Dell'Anna, Mol. Catal. 446, 31 (2018); https://doi.org/10.1016/j.mcat.2017.12.015
[20] B. Huang, W. Qian, C. Yu, T. Wang, G. Zeng, C. Lei, Chem. Eng. J. 306, 607 (2016); https://doi.org/10.1016/j.cej.2016.07.109
[21] X. Wang, N. Perret, M.A. Keane, Chem. Eng. J. 210, 103 (2012); https://doi.org/10.1016/j.cej.2012.08.061
[22] M. Wang, B. Feng, H. Li, H. Li, Chem. 5, 805 (2019); https://doi.org/10.1016/j.chempr.2019.01.003
[23] Q. Zhang, K. Li, Y. Xiang, Y. Zhou, Q. Wang, L. Guo, L. Ma, X. Xu, C. Lu, F. Feng, J. Lv, J. Ni, X. Li, Appl. Catal. A Gen. 581, 74 (2019); https://doi.org/10.1016/j.apcata.2019.05.016
[24] C. Lu, Q. Zhu, X. Zhang, H. Ji, Y. Zhou, H. Wang, Q. Liu, J. Nie, W. Han, X. Li, ACS Sustain. Chem. Eng. 7, 8542 (2019); https://doi.org/10.1021/acssuschemeng.9b00322
[25] Q. Zhang, W. Xu, X. Li, D. Jiang, Y. Xiang, J. Wang, J. Cen, S. Romano, J. Ni, Appl. Catal. A Gen. 497, 17 (2015); https://doi.org/10.1016/j.apcata.2015.02.043
[26] M. Takasaki, Y. Motoyama, K. Higashi, S.-H. Yoon, I. Mochida, H. Nagashima, Org. Lett. 10, 1601 (2008); https://doi.org/10.1021/ol800277a
[27] A. Finiels, P. Geneste, C. Moreau, J. Mol. Catal. A Chem. 107, 385 (1996); https://doi.org/10.1016/1381-1169(95)00237-5
[28] X. Yan, J. Sun, Y. Wang, J. Yang, J. Mol. Catal. A Chem. 252, 17 (2006); https://doi.org/10.1016/j.molcata.2006.01.060
[29] C. Moreau, C. Saenz, P. Geneste, M. Breysse, M. Lacroix, "Studies in Surface Science and Catalysis: Heterogeneous Catalysis and Fine Chemicals II ", Elsevier, Amsterdam, Netherlands, 121 (1991); https://doi.org/10.1016/S0167-2991(08)61112-X
[30] M. V. Landau, Sol-Gel Processing, "Synthesis of Solid Catalysts", Wiley-VCH Verlag GmbH & Co. KGaA, Weinheim, Germany, 83 (2009); https://doi.org/10.1002/9783527626854.ch5
[31] D. Nunes, A. Pimentel, L. Santos, P. Barquinha, L. Pereira, E. Fortunato, R. Martins, Metal Oxide Nanostructures: Synthesis, Properties and Applications, Elsevier, Amsterdam, Netherlands,

21 (2019); https://doi.org/10.1016/B978-0-12-811512-1.00002-3

[32] E. Marceau, X. Carrier, M. Che, "Synthesis of Solid Catalysts: Impregnation and Drying", Wiley-VCH Verlag GmbH & Co. KGaA, Weinheim, Germany, 59 (2009); https://doi.org/10.1002/9783527626854.ch4

[33] F. Cárdenas-Lizana, D. Lamey, N. Perret, S. Gómez-Quero, L. Kiwi-Minsker, M.A. Keane, Catal. Commun. 21, 46 (2012); https://doi.org/10.1016/j.catcom.2012.01.027

[34] M.A. Keane, Appl. Catal. A Gen. 271, 109 (2004); https://doi.org/10.1016/j.apcata.2004.02.051

[35] G. Tavoularis, M.A. Keane, J. Chem. Technol. Biotechnol. 74, 60 (1999); https://doi.org/10.1002/(SICI)1097-4660(199901)74:1<60::AID-JCTB992>3.0.CO;2-K

[36] D. Mateos, B. Valdez, J.R. Castillo, N. Nedev, M. Curiel, O. Perez, A. Arias, H. Tiznado, Ceram. Int. 45, 11403 (2019); https://doi.org/10.1016/j.ceramint.2019.03.005

[37] M. Gousi, C. Andriopoulou, K. Bourikas, S. Ladas, M. Sotiriou, C. Kordulis, A. Lycourghiotis, Appl. Catal. A Gen. 536, 45 (2017); https://doi.org/10.1016/j.apcata.2017.02.010

[38] V.R.S. Cassimiro, R.C. Monteiro, R. Bacani, L.M. Toscani, D.G. Lamas, S.A. Larrondo, M.C.A. Fantini, Ceram. Int. 45, 19617 (2019); https://doi.org/10.1016/j.ceramint.2019.06.209

[39] L.-F. Zhai, S.-Y. Kong, M.-F. Duan, M. Sun, J. Clean. Prod. 224, 256 (2019); https://doi.org/10.1016/j.jclepro.2019.03.228

[40] A. Morales-Marín, J.L. Ayastuy, U. Iriarte-Velasco, M.A. Gutiérrez-Ortiz, Appl. Catal. B Environ. 244, 931 (2019); https://doi.org/10.1016/j.apcatb.2018.12.020

[41] C. Zhang, X. Hu, Z. Zhang, L. Zhang, D. Dong, G. Gao, R. Westerhof, S.S.A. Syed-Hassan, Fuel 227, 307 (2018); https://doi.org/10.1016/j.fuel.2018.04.111

[42] J. Oudar, Catal. Rev. 22, 171 (1980); https://doi.org/10.1080/03602458008066533